Robust Stability Analysis of Voltage and Current Control for Distributed Generation Systems

Mohammad N. Marwali, *Member IEEE*, Min Dai, *Student Member*, *IEEE*, and Ali Keyhani, *Fellow*, *IEEE*

***Abstract* – This paper analyzes the robust stability of a voltage and current control solution for a stand-alone distributed generation (DG) unit using structured singular value or μ-framework based method. The voltage and current control solution consists of a discrete-time sliding mode (DSM) current controller and a perfect Robust Servomechanism Problem (RSP) voltage controller, which has been shown effective in transient response and harmonic minimization in previous study without considering parametric uncertainty. The stability robustness of the system and its transient performance are investigated under various tuning parameters of the controller. The analysis results presented in this paper demonstrate that the controller parameters can be tuned and verified to satisfy a certain transient performance requirement and at the same time guarantee robust stability under system parameter uncertainties and load variations.**

***Index terms* – pulse width modulated inverters, digital signal processors (DSP), robust stability, structured singular value.**

I. INTRODUCTION

A feedback control system is said to achieve robust stability if it remains stable for all considered perturbations in the plant. The stability robustness of the system is evaluated by its tolerance to perturbations. In feedback controlled PWM inverter systems, e.g., an inverter based three-phase distributed generation (DG) unit operated in stand-alone mode, load disturbance, noise, and parametric uncertainty of the electrical components in the circuit are the major plant perturbations that have significant impacts on both system stability and performance and therefore warrant detailed investigation. Robust stability related topics about PWM inverter based systems have been addressed in literature. Czarkowski et al. [1] have studied a state feedback control method of a PWM dc-dc converter for its robust stability under parametric uncertainty. This study uses the Kharitonov's theorem [2] which checks whether the feedback system is stable by applying the Routh-Hurwitz stability tests but does not tell the stability margin or how stable the system is. Grundling et al. [3] have developed a robust model reference adaptive control technique for uninterruptible power supplies (UPS) which was expected to handle model inaccuracy but no robust stability property of the technique was presented. Lee et al. [4] have proposed an H_∞ loop-shaping robust controller design technique for UPS with robust stability analysis. However, this technique does not perform well under nonlinear load, which significantly undermines its value for power supply applications. Lin et al. [5] have designed a dc-dc power converter controller using structured singular value (μ) concept, which evaluates how stable the system is under the worst case of perturbation. This study uses admittance instead of resistance to model the dc load, which is proved convenient in the analysis. However, this design only considers load disturbances and no parametric uncertainties are included in the perturbation. Mohamed [6] has proposed a robust controller for a current source inverter (CSI) fed induction motor drive. Both H_∞ loop-shaping and μ-analysis techniques are applied in the research but no parametric uncertainty is considered which undermines the strength. Ye et al. [7] have proposed a robust controller design method for high frequency resonant inverters. This approach applies H_∞ robust controller synthesis method provided in Matlab® Robust Control Toolbox but only includes load and external input voltage in the perturbation.

A perfect Robust Servomechanism Problem (RSP) controller has been developed in [8], which guarantees exact asymptotic tracking of the fundamental frequency reference and error regulation of the load disturbance at each of the harmonic frequency included in the servo compensators. The perfect RSP guarantees this property independent of any perturbations in the plant as long as they do not destabilize system. The perfect RSP guarantees stability under nominal plant without perturbation, however the stability under perturbation is not guaranteed and this issue is not addressed in [8]. Therefore, it is important to analyze the stability property of the controller under possible disturbances in order to ensure proper operation of the converter over its intended operating range.

In this paper, the stability robustness of the system with the controller developed in [8] will be investigated using *structured singular values* or *μ-framework.* Specifically, perturbations due to load variations and parameters uncertainties of the system components are considered. A linear quadratic cost function with separate weighting scalars for plant states and servo compensator states have been used to find solutions to the perfect RSP. In this paper, the stability robustness and transient response of the resulting control system will be investigated for different choices of these weighting scalars. The transient performance of the system is evaluated by performing moving window RMS calculations of the three phase output voltages under transient load change from zero to 100% resistive load.

A review of the voltages and current controller developed in [8] is first presented followed by a summary of robust stability theory using structured singular value or μ-framework. The

M. N. Marwali is with Liebert Corporation, Delaware, Ohio, USA (e-mail: nanda_marwali@liebert.com).

M. Dai and A. Keyhani are with the Department of Electrical and Computer Engineering, The Ohio State University, Columbus, Ohio, USA (e-mail: {dai.21, keyhani.1}@osu.edu).

This research is supported in part by the National Science Foundation under the grants NSF ECS 0501349 and ECS 0105320.

uncertainty model is then developed and used for verifying the robust stability of the system.

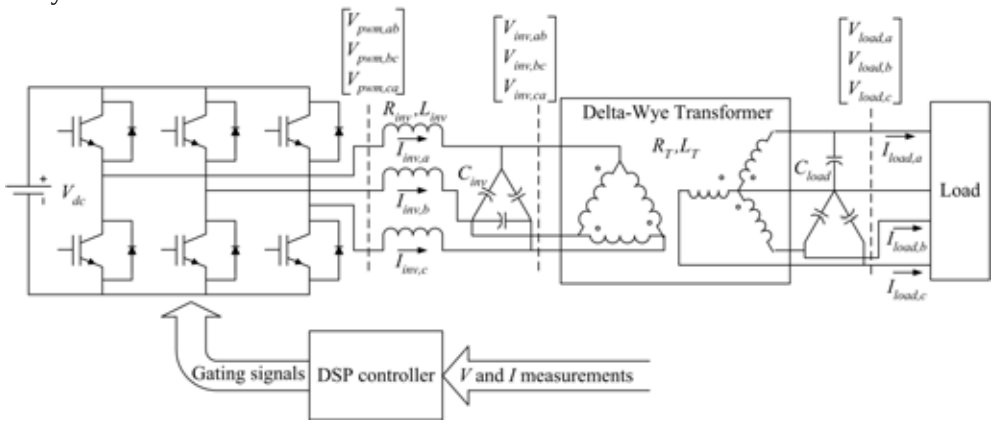

Fig. 1 PWM inverter based DG system in stand-alone mode.

II. VOLTAGES AND CURRENTS CONTROL

Fig. 1 shows a PWM inverter used for the DG system, where a constant dc voltage source is used to approximate most typical distributed generation sources, such as fuel cell, photovoltaic, wind, and microturbine generation systems. This approximation is surely reasonable when these sources work together with a stiff voltage regulation and secondary energy storage when necessary, such as the systems shown in [9] and [10]. The approximation is also reasonable even with an unregulated DC bus due to the adaptability of the PWM inverter as long as the DC voltage is high enough to generate the control command.

The DG system shown in Fig. 1, if operated in standalone mode, is typically used as standalone on-site power or standby emergency power when the utility grid is not available or the utility power is accidentally lost due to fault.

A state space model of the system in DQ0 stationary reference using per-unit notation can be developed and is given by (1) [11].

$$d\vec{v}inv_{qd}/dt = \left(\vec{i}\,inv_{qd} - \cdot\vec{i}\,snd'_{qd}\right)/c_{inv} \quad (1.a)$$

$$d\vec{i}\,inv_{qd}/dt = \left(-r_{inv}\cdot\vec{i}\,inv_{qd} - \vec{v}inv_{qd} + \vec{v}pwm_{qd}\right)/l_{inv} \quad (1.b)$$

$$d\vec{v}load'_{qd}/dt = \left(\vec{i}\,snd'_{qd} - \vec{i}\,load'_{qd}\right)/c_{load} \quad (1.c)$$

$$d\vec{i}\,snd'_{qd}/dt = \left(-r_T\cdot\vec{i}\,snd'_{qd} + \vec{v}inv_{qd} - \vec{v}load'_{qd}\right)/l_T \quad (1.d)$$

$$dvload_0/dt = \left(isnd_0 - iload_0\right)/c_{load} \quad (1.e)$$

$$disnd_0/dt = \left(-r_T\cdot isnd_0 - vload_0\right)/c_{load} \quad (1.f)$$

where the following per-unit capacitances, inductances, and resistances are defined from their corresponding per-unit values:

$$c_{inv} \equiv 1/\left(\omega_f\cdot xc_{inv}\right);\ c_{load} \equiv 1/\left(\omega_f\cdot xc_{load}\right);\ l_{inv} \equiv xl_{inv}/\omega_f,$$

$$l_{trans} \equiv xl_T/\omega_f;\ r_{inv} \equiv xr_{inv};\ r_T \equiv xr_T$$

The per-unit values of the capacitances, inductances, and resistances are calculated from:

$$xl_{inv} \equiv \omega_f L_{inv}/Z1,\ xr_{inv} \equiv R_{inv}/Z1,\ xc_{inv} \equiv 1/\left(\omega_f 3C_{inv}\right)/Z1,$$

$$xl_T \equiv \omega_f L_T/Z2,\ xr_T \equiv R_T/Z2,\ xc_{load} \equiv 1/\left(\omega_f C_{load}\right)/Z2$$

where the base impedances $Z1$ and $Z2$ are defined as:

$$Z1 \equiv V1/I1 \qquad Z2 \equiv V2/I2$$

with $V1$ and $V2$ denote the rated line-to-neutral primary and secondary transformer voltages, and $I1$ and $I2$ denote the rated primary and secondary currents, respectively. The voltages and currents in equations (1) are the DQ0 stationary reference frame variables of the per-unit voltages and currents in ABC given as:

$$\vec{v}pwm_{abc} = \vec{V}pwm_{abc}/V1,\quad \vec{v}inv_{abc} = \vec{V}inv_{abc}/V1$$

$$\vec{i}\,inv_{abc} = \vec{I}inv_{abc}/I1,\quad \vec{v}load_{abc} = \vec{V}load_{abc}/V2$$

$$\vec{i}\,load_{abc} = \vec{I}load_{abc}/I1$$

where the actual ABC voltages and currents are defined as follows:

$$\vec{V}pwm_{abc} = \left[Vpwm_{ab}\quad Vpwm_{bc}\quad Vpwm_{ca}\right]^T/\sqrt{3}$$

$$\vec{V}inv_{abc} = \left[Vinv_{ab}\quad Vinv_{bc}\quad Vinv_{ca}\right]^T/\sqrt{3}$$

$$\vec{V}load_{abc} = \left[Vload_a\quad Vload_b\quad Vload_c\right]^T,$$

$$\vec{I}load_{abc} = \left[Iload_a\quad Iload_b\quad Iload_c\right]^T$$

$$\vec{I}snd_{abc} = \left[Isnd_a\quad Isnd_b\quad Isnd_c\right]^T,$$

$$\vec{I}inv_{abc} = \left[Iinv_a - Iinv_b,\quad Iinv_b - Iinv_c,\quad Iinv_c - Iinv_a\right]^T/\sqrt{3}$$

The following changes of variables have been used for the secondary transformer currents, load currents, and load voltages in (1):

$$\vec{i}\,snd'_{qd} = tri_{qd}\cdot\vec{i}\,snd_{qd} \quad (2.a)$$

$$\vec{i}\,load'_{qd} = tri_{qd}\cdot\vec{i}\,load_{qd} \quad (2.b)$$

$$\vec{v}load'_{qd} = trv_{qd}^{-1}\cdot\vec{v}load_{qd} \quad (2.c)$$

with matrices tri_{qd} and trv_{qd} defined as:

$$tri_{qd} = \left[K_s\cdot tr_i\cdot K_S^{-1}\right]_{col1,2}^{row1,2} = \begin{bmatrix}-1 & 0\\ 0 & -1\end{bmatrix} \quad (3.a)$$

$$trv_{qd} = \left[K_s\cdot tr_v\cdot K_S^{-1}\right]_{col1,2}^{row1,2} = \begin{bmatrix}-1 & 0\\ 0 & -1\end{bmatrix} \quad (3.b)$$

Matrices tr_i and tr_v in (3) denote currents and voltages transformations of a particular delta-wye transformer, e.g.:

$$tr_i = \frac{1}{3}\begin{bmatrix}-2 & 1 & 1\\ 1 & -2 & 1\\ 1 & 1 & -2\end{bmatrix},\qquad tr_v = \begin{bmatrix}-1 & 0 & 0\\ 0 & -1 & 0\\ 0 & 0 & -1\end{bmatrix}$$

From equations (1) it can be seen that the zero variables are not affected by the control inputs, and therefore need not be considered in the controller design. Moreover, the D and Q axis are completely decoupled and have the same dynamics. Therefore, a controller can be developed and analyzed for one of the *dq* axis and the same controller can be used for the other.

Fig. 2 shows the voltages and currents control developed in [8]. An RSP controller is used for the voltage control and a discrete-time sliding mode (DSM) controller is used for the current control.

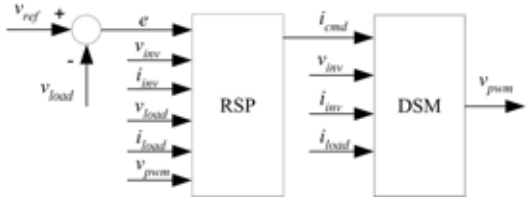

Fig. 2 The RSP and DSM controllers.

The DSM controller is used in the current loop to limit the inverter current under overload condition because of the fast and no overshoot response it provides. Suppose a discrete form of the LC filter dynamics given in equations of (1.a) and (1.b) are given by:

$$\vec{x}_1(k+1) = A_1^* \vec{x}_1(k) + B_1^* \vec{u}(k) + E_1^* \vec{d}_1(k) \tag{4}$$

where the states are $\vec{x}_1 = \left[\vec{v}inv, \vec{i}inv\right]$, the inputs $u = vpwm$ and disturbances $\vec{d}_1 = isnd$. Note the subscript *dq* has been dropped since the controller is designed for one axis but apply for both. To force the inverter currents to follow their commands, the sliding mode surface is chosen as: $s(k) = C_1 \cdot \vec{x}_1(k+1) - icmd(k)$ where $C_1 \cdot \vec{x}_1(k+1) = iinv(k+1)$, so that when discrete sliding mode occurs, we have $\vec{s}(k) = 0$ or $iinv(k+1) = icmd(k)$. The existence of the discrete sliding mode can then be guaranteed if the control is given by:

$$vpwm(k) = \left(C_1 B_1^*\right)^{-1}\left(\vec{i}cmd - C_1 A_1^* \vec{x}_1(k) - C_1 E_1^* \vec{d}_1(k)\right) \tag{5}$$

The RSP is adopted for voltage control due to its capability to perform zero steady state tracking error under unknown load and eliminate harmonics of any specified frequencies with guaranteed system stability for nominal plant parameters and load variations. The theory behind the RSP is based on the solution of robust servomechanism problem [12] where the internal model principle [13] and the optimal control theory for linear systems are combined. The RSP controller consists of a discrete form of the continuous servo compensator:

$$\dot{\vec{\eta}} = A_c \vec{\eta} + B_c e_V, \qquad e_V = Vref - Vload \tag{6}$$

where

$$\vec{\eta} = \left[\vec{\eta}_1, \vec{\eta}_2, \cdots \vec{\eta}_n\right]^T \quad \vec{\eta}_i \in R^2, \quad i = 1,2,\ldots n$$

$$A_c = \text{block diag}\left[Ac_1, Ac_2, \cdots, Ac_n\right]$$

$$B_c = \left[Bc_1, Bc_2, \cdots, Bc_n\right]^T$$

with

$$Ac_i = \begin{pmatrix} 0 & 1 \\ -\omega_i^2 & 0 \end{pmatrix}, \quad i = 1,2,\ldots n$$

$$Bc_i = \begin{pmatrix} 0 & 1 \end{pmatrix}^T, \; i = 1,2,\ldots n$$

Note that each of the blocks $\dot{\vec{\eta}}_i = Ac_1 \vec{\eta}_i + Bc_i \vec{e}_{Vqd}$ represents a state space implementation of the continuous transfer function: $1/\left(s^2 + \omega_i^2\right)$ where each $\omega_i = 2\pi f_i$ represents the fundamental frequency to track and each of the harmonic frequencies to be eliminated. For a 60-Hz DG system with desire to eliminate 5th and 7th harmonics, for example, we use $\omega_1 = 2\pi \cdot 60$, $\omega_2 = 2\pi \cdot 5 \cdot 60$, and $\omega_3 = 2\pi \cdot 7 \cdot 60$

To design the *voltage controller* using the perfect RSP, we need to consider a combination of the true plant in (1) and the discrete time sliding mode current controller (5) as the equivalent 'plant' seen by the outer voltage loop. Assuming a discrete form of (1) given by $\vec{x}_p^*(k+1) = A_p^* \vec{x}_p^*(k) + B_p^* vpwm(k)$, the augmented true plant and discrete sliding mode current controller can be found as in

$$\vec{x}_p^*(k+1) = A_d \vec{x}_p^*(k) + B_d \cdot icmd(k) \tag{7}$$

with

$$A_d = A_p^* - B_p^*\left(C_1 B_1^*\right)^{-1}\left(B_1^* C_{11} + E_1^* C_{12}\right)$$

$$B_d = B_p^*\left(C_1 B_1^*\right)^{-1}$$

$$C_{11} = \begin{bmatrix} 1 & 0 & 0 & 0 & 0 \\ 0 & 1 & 0 & 0 & 0 \end{bmatrix}$$

$$C_{12} = \begin{bmatrix} 0 & 0 & 0 & 1 & 0 \end{bmatrix}$$

The complete perfect RSP voltage controller is given by states feedback:

$$icmd(k) = K_0 x_p^*(k) + K_1 \eta(k) \tag{8}$$

where the gains $K = \begin{bmatrix} K_0 & K_1 \end{bmatrix}$ are found by minimizing a certain linear quadratic cost function for the augmented 'equivalent plant' (7) and a discrete form of the servo compensator (6):

$$\begin{bmatrix} \vec{x}_p^*(k+1) \\ \eta(k+1) \end{bmatrix} = \begin{bmatrix} A_d & 0 \\ -B_c^* C & A_c^* \end{bmatrix} \begin{bmatrix} \vec{x}_p^*(k) \\ \eta(k) \end{bmatrix} + \begin{bmatrix} B_d \\ -B_c^* D \end{bmatrix} u_1(k) \tag{9}$$

To achieve desired transient performance and guarantee robust stability under plant uncertainties, the following linear quadratic cost function has been used in this paper:

$$J_\varepsilon = \sum_{k=0}^{\infty} \begin{pmatrix} w_p \cdot x_p^*(k)' \cdot x_p^*(k) + w_{S1} \cdot \eta_1(k)' \cdot \eta_1(k) \\ + w_{SH} \sum_h \eta_h(k)' \cdot \eta_h(k) + \varepsilon \cdot u(k)' u(k) \end{pmatrix} \tag{10}$$

where w_p, w_S and w_{SH} represent weighting scalars for plant states (x_p^*), fundamental servo compensator states (η_1), and harmonics servo compensator states (η_h). Solution to this linear quadratic optimization problem is well known and can be found using Matlab command *dlqr* [14].

The effectiveness of the technique can be demonstrated by experimental results shown in Fig. 3, which exhibits well regulated sinusoidal output voltage waveforms under various types of load.

III. ROBUST STABILITY ANALYSIS USING STRUCTURED SINGULAR VALUE μ

Structured Singular Value μ can be used to analyze and evaluate the stability robustness of a Multi-Input-Multi-Output (MIMO) linear system under structured perturbations. In order to use the *μ-framework* to analyze robust stability of a linear system under perturbation, the problem needs to be recast into a feedback loop diagram of Fig. 3 where M represents a known stable MIMO transfer function of the linear system with n inputs and n outputs and Δ a structured uncertainty matrix of the form (11) [15,16]:

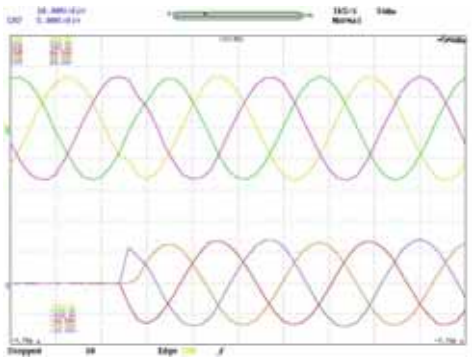

(a)

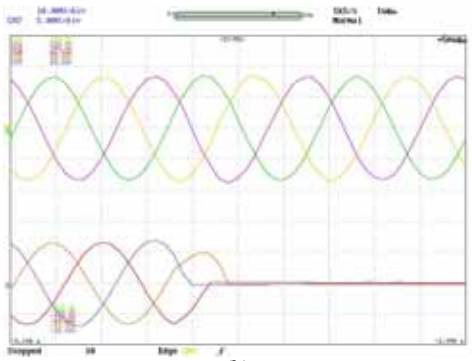

(b)

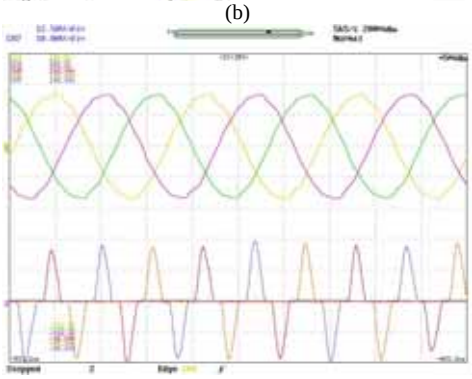

(c)

Fig. 3 Experimental results of the standalone DG system under different scenarios, where the top traces are three-phase output voltages and the bottom traces are three-phase load currents - (a) transient response at load stepping up from 0 to 100%; (b) transient response at load stepping down from 100% to 0; (c) steady state performance under three-phase nonlinear load.

$$\mathbf{\Delta} = \left\{ diag\left[\delta_1 I_{r1}, \ldots \delta_s I_{rs}, \Delta_1 \ldots \Delta_F\right] : \delta_i \in C, \Delta_j \in C^{m_j x m_j} \right\} \qquad (11)$$

where $\sum_{i=1}^{S} r_i + \sum_{j=1}^{F} m_j = n$.

The structured singular value of M with respect to the uncertainty set $\mathbf{\Delta}$ is defined as:

$$\mu_{\Delta}(M) = \frac{1}{\min\{\bar{\sigma}(\Delta) : \Delta \in \mathbf{\Delta}, \det(I - M\Delta) = 0\}}$$

The Generalized Small-Gain Theorem provides robust stability result of the system using the structured singular value. It states that, if nominal $M(s)$ is stable then the perturbed system $(I - M\Delta)^{-1}$ is stable for all stable Δ_i for which $\|\Delta_i\|_{\infty} \le 1$ if and only if $\mu_{\Delta}(M(j\omega)) < 1$ for all $\omega \in R$ [15, 16].

A. Uncertain Open-Loop Model

In order to use the μ-framework to analyze robust stability, the problem needs to be recast to that of Fig. 4. A class of general feedback loops called *linear fractional transformations* (LFT) can be used to achieve this. For complete discussion of the LFT and its use in representing model uncertainties, refer to [15]. Using the state space model (1), a single-phase equivalent circuit of the converter with RL load can be derived as shown in Fig. 5. This represents the open-loop model of the plant.

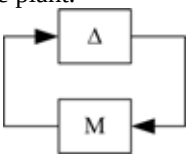

Fig. 4 Representation of a linear system with uncertainties.

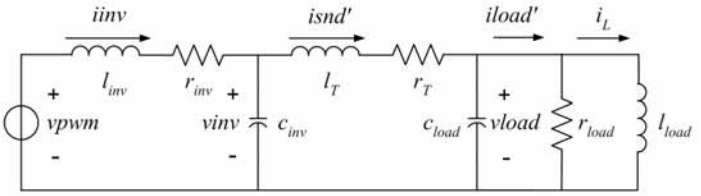

Fig. 5 Open loop model of the nominal plant.

The dynamic equations of the plant are given by

$$dvinv/dt = (iinv - \cdot isnd')/c_{inv} \qquad (12.a)$$

$$diinv/dt = (-r_{inv} \cdot iinv - vinv + vpwm)/l_{inv} \qquad (12.b)$$

$$dvload/dt = (isnd'_{snd} - g_{load} vload' - i_L)/c_{load} \qquad (12.c)$$

$$disnd'/dt = (-r_T \cdot isnd' + vinv - vload')/l_T \qquad (12.d)$$

$$di_L/dt = \lambda_{load} vload' \qquad (12.e)$$

$$i'_{load} = g_{load} v'_{load} + i_L \qquad (12.f)$$

where $g_{load}=1/r_{load}$ is the per-unit conductance of the load and $\lambda_{load} = 1/l_{load}$ is the inverse of the per-unit load inductance.

Let us assume that the following parameter variations exist in the system due to manufacturing tolerances of the components used and/or errors in the parameters identification processes:

- Inverter filter capacitor tolerance: ±6%
- Inverter filter inductor tolerance: ±15%
- Inverter filter inductor losses tolerance: ±50%
- Output filter capacitor tolerance: ±6%
- Transformer filter inductor tolerance: ±15%
- Transformer filter inductor losses tolerance: ±50%

Furthermore, the specification of the unit requires that it operates stably without degradation in performance for load from zero to 200% with power factor of 0.8 lagging at maximum load. This specification represents variation of the resistive load from zero to 160%, and inductive load from zero to 120%.

The above parameter variations due to manufacturing tolerances and load variations can be precisely written as follows:

$$c_{inv} = c_{inv0}\left(1+\tau_{cinv}\cdot\delta_{cinv}\right),\ |\delta_{cinv}|<1 \quad (13.a)$$

$$l_{inv} = l_{inv0}\left(1+\tau_{linv}\cdot\delta_{linv}\right),\ |\delta_{linv}|<1 \quad (13.b)$$

$$c_{load} = c_{load0}\left(1+\tau_{cload}\cdot\delta_{cload}\right),\ |\delta_{cload}|<1 \quad (13.c)$$

$$l_{T} = l_{T0}\left(1+\tau_{lT}\cdot\delta_{lT}\right),\ |\delta_{lT}|<1 \quad (13.d)$$

$$r_{inv} = r_{inv0}\left(1+\tau_{rinv}\cdot\delta_{rinv}\right),\ |\delta_{rinv}|<1 \quad (13.e)$$

$$r_{T} = r_{T0}\left(1+\tau_{rT}\cdot\delta_{rT}\right),\ |\delta_{rT}|<1 \quad (13.f)$$

$$g_{load} = g_{load0}\left(1+\tau_{gload}\cdot\delta_{gload}\right),\ |\delta_{gload}|<1 \quad (13.g)$$

$$\lambda_{load} = \lambda_{load0}\left(1+\tau_{\lambda load}\cdot\delta_{\lambda load}\right),|\delta_{\lambda load}|<1 \quad (13.h)$$

where the terms with subscript zero indicate the nominal values of the parameters and τ terms denote their percentage tolerances given above. The following load parameters can be used to represent the desired load variation above: $g_{load0}=0.8$, $\lambda_{load0}=0.6\omega_f$ with $\tau_{gload}=\tau_{\lambda load}=1.0$.

Parameters c_{inv}, l_{inv}, c_{load}, and l_T appear in denominators in (12) and can be represented using lower LFT similar to that shown in Fig. 6(a) for $1/c_{inv}$. LFTs for r_{inv}, r_T, r_{load}, and λ_{load} are constructed similar to that of Fig. 6(b) for r_{inv}, where

$$dr_{inv} = r_{inv0}\cdot\tau_{rinv}, \quad (14.a)$$

$$dr_{T} = r_{T0}\cdot\tau_{rT}, \quad (14.b)$$

$$dg_{load} = g_{load0}\cdot\tau_{gload}, \text{ and} \quad (14.c)$$

$$d\lambda_{load} = \lambda_{load0}\cdot\tau_{\lambda load}, \quad (14.d)$$

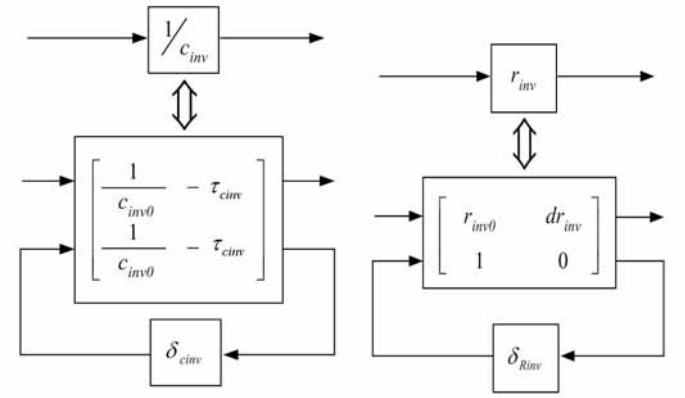

(a) (b)

Fig. 6 LFTs for (a) $1/c_{inv}$- inverse term (b) r_{inv} - non-inverse term.

For each uncertain term, the corresponding LFT as in Fig. 6 can be substituted into the dynamic model of equation (12) as shown in Fig. 7 with the uncertain perturbation (δ) blocks separately represented by $\Delta(s)$ as shown in Fig. 8, where $\Delta(s)$ is given by $\{\delta_{Cinv}, \delta_{Linv}, \delta_{Cload}, \delta_{LT}, \delta_{Rinv}, \delta_{RT}, \delta_{Gload}, \delta_{\lambda load}\}$. The block $P(s)$ in Fig. 8 contains all the known model information of the plant and will be referred to as the nominal open-loop plant model. The combination of $P(s)$ and $\Delta(s)$ forms the uncertain open-loop model.

The state space model of the nominal plant P can be derived by inspection of Fig. 7 with the following states, inputs, and outputs variables:

States: $X = \left[v_{inv} \quad i_{inv} \quad v_{load} \quad i_{snd} \quad i_L\right]^T$.

Inputs: $U = \left[v_{pwm} \quad W^T\right]^T$, where

$W = \left[w_{cinv} \quad w_{linv} \quad w_{cload} \quad w_{lT} \quad w_{rinv} \quad w_{rT} \quad w_{gload} \quad w_{\lambda load}\right]^T$.

Outputs: $Y = \left[v_{inv} \quad i_{inv} \quad v_{load} \quad i_{load} \quad Z^T\right]^T$, where

$Z = \left[z_{cinv} \quad z_{linv} \quad z_{cload} \quad z_{lT} \quad z_{rinv} \quad z_{rT} \quad z_{gload} \quad z_{\lambda load}\right]^T$.

The state space equations are given as:

$$\dot{X} = A_P X + B_P U$$
$$Y = C_P X + D_P U \quad (15)$$

where

$$A_P = \left[A_{nom}\right],\ B_P = \left[B_{nom} \quad B_{del}\right],\ C_P = \begin{bmatrix} C_{nom} \\ C_{del} \end{bmatrix},\ D_P = \begin{bmatrix} D_{nom} \\ D_{del} \end{bmatrix}.$$

The terms with subscription *nom* are the nominal model parameters derived from (12) and the ones with subscription *del* are defined in (16), (17), and (18), respectively.

B. Uncertain Closed-Loop Model

In order to use the μ-framework to analyze the robust stability of the system, the system needs to be recast in to that of Fig. 4. In this case, the system M comprises of the nominal open loop plant $P(s)$ and the controller loop closed around it as illustrated in Fig. 8 where the vectors X, W, and Z as defined above. Matlab with its Control System Toolbox [14] and μ-Analysis and Synthesis Toolbox [15], has been utilized to achieve this purpose.

Since the controller is implemented in the discrete time system, the following steps are necessary to obtain the closed loop plant model:

1. Apply a Zero Order Hold transformation to the continuous plant P, to include the effect of the sample and hold process of the digital sampling process.
2. Transform the discretized plant back to continuous system in the *w-plane* by applying an inverse Tustin transformation. This transformation has the property of preserving the frequency response of the discrete time systems
3. Obtain state space representations of the *RSP* and Discrete Sliding Mode controller with inputs and outputs definitions as shown in Fig. 2. The combined controller state-space system can be calculated using *sysic* (μ-Toolbox) command in Matlab [15]

4. The combined controller system is then transformed into the *w-plane* in continuous domain using the inverse Tustin transformation
5. Finally, the closed loop plant model *M* is obtained by invoking the Matlab *sysic* command for the transformed nominal plant model from step 2 and the controller system obtained in step 4.

$$B_{del} = \begin{bmatrix} -\tau_{cinv} & 0 & 0 & 0 & 0 & 0 & 0 & 0 \\ 0 & -\tau_{linv} & 0 & 0 & \frac{-dr_{inv}}{l_{inv0}} & 0 & 0 & 0 \\ 0 & 0 & -\tau_{cload} & 0 & 0 & 0 & \frac{-dg_{load}}{c_{load0}} & 0 \\ 0 & 0 & 0 & -\tau_{IT} & 0 & \frac{-dr_T}{l_{T0}} & 0 & 0 \\ 0 & 0 & 0 & 0 & 0 & 0 & 0 & d\lambda_{loadl} \end{bmatrix} \tag{16}$$

$$C_{del} = \begin{bmatrix} 0 & \frac{1}{c_{inv0}} & 0 & \frac{-1}{c_{inv0}} & 0 \\ \frac{-1}{l_{inv0}} & \frac{-r_{inv0}}{l_{inv0}} & 0 & 0 & 0 \\ 0 & 0 & \frac{-g_{load0}}{c_{load0}} & \frac{1}{c_{load0}} & \frac{-1}{c_{load0}} \\ \frac{1}{l_{T0}} & 0 & \frac{-1}{r_{T0}} & \frac{-r_{T0}}{r_{T0}} & 0 \\ 0 & 1 & 0 & 0 & 0 \\ 0 & 0 & 0 & 1 & 0 \\ 0 & 0 & 1 & 0 & 0 \\ 0 & 0 & 1 & 0 & 0 \end{bmatrix} \tag{17}$$

$$D_{del} = \begin{bmatrix} 0 & -\tau_{cinv} & 0 & 0 & 0 & 0 & 0 & 0 & 0 \\ \frac{1}{l_{inv0}} & 0 & -\tau_{linv} & 0 & 0 & \frac{-dr_{inv}}{l_{inv0}} & 0 & 0 & 0 \\ 0 & 0 & 0 & -\tau_{cload} & 0 & 0 & \frac{-dg_{load}}{c_{load0}} & 0 & 0 \\ 0 & 0 & 0 & 0 & -\tau_{IT} & \frac{-dr_T}{l_{T0}} & 0 & 0 & 0 \\ 0 & 0 & 0 & 0 & 0 & 0 & 0 & 0 & 0 \\ 0 & 0 & 0 & 0 & 0 & 0 & 0 & 0 & 0 \\ 0 & 0 & 0 & 0 & 0 & 0 & 0 & 0 & 0 \\ 0 & 0 & 0 & 0 & 0 & 0 & 0 & 0 & 0 \end{bmatrix} \tag{18}$$

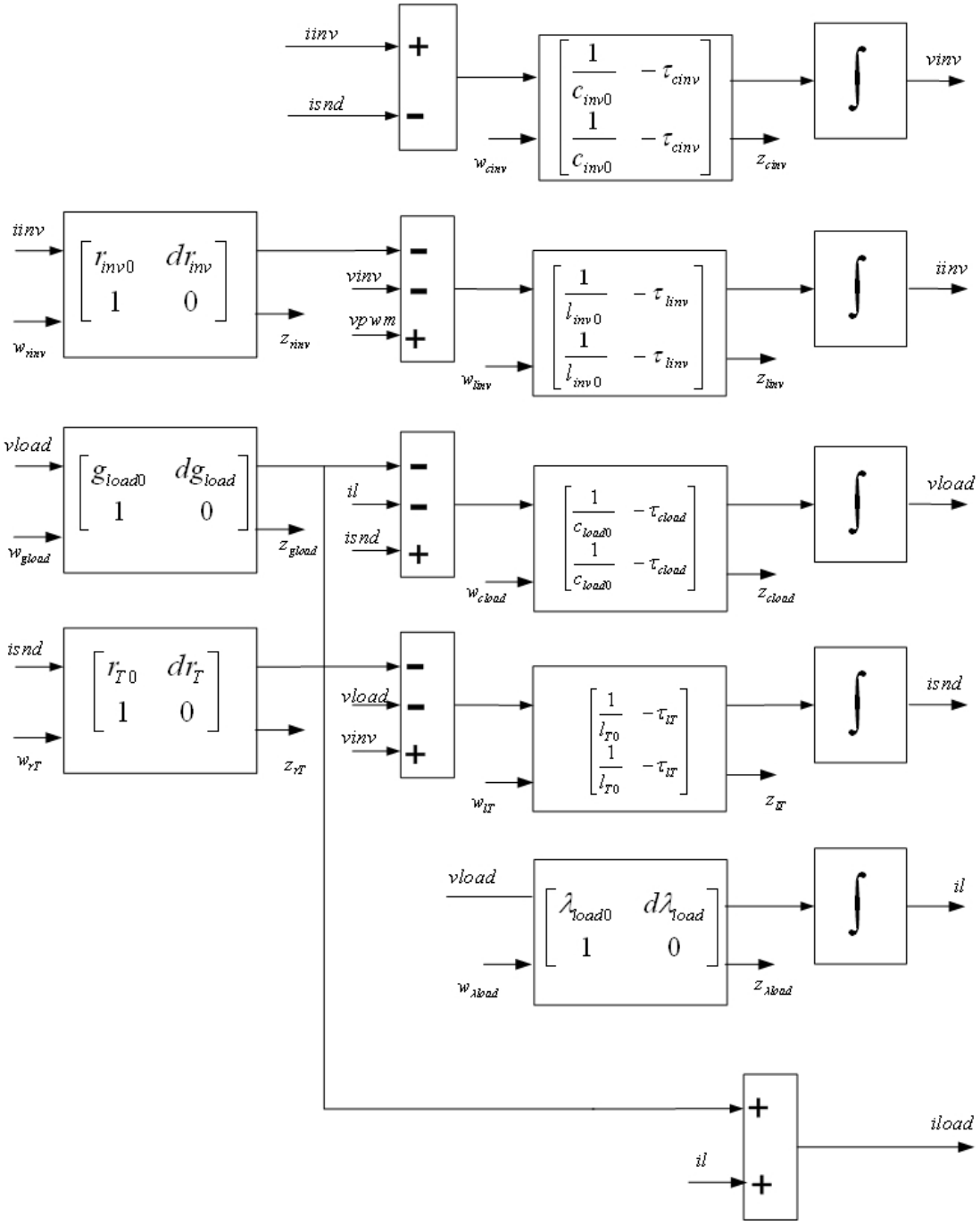

Fig. 7 Block diagram of the nominal plant $P(s)$ with LFTs of the uncertain parameters.

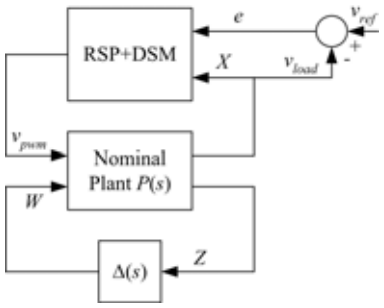

Fig. 8 Uncertain closed-loop model.

IV. TUNING THE CONTROLLER PERFORMANCE

Recall earlier that the w_p, w_S, and w_{SH} in cost function (10) are the weighting scalars for the plant states, fundamental, and harmonic servo compensator states respectively. The selection of values of these scalars provides a way of tuning the controller for desired transient performance and stability robustness. The structured singular value discussed in the previous sections will be used to evaluate the robust stability of each controller resulting from different choices of weighting scalars. A time response simulation of the single-phase equivalent circuit will be used to compare the transient performance of each controller. To quantify the transient

performance, it is common in the industry to use the deviation of the RMS output voltage from its nominal value during a 100% resistive load change as a performance measure. A less than 5% deviation of output voltage under 100% resistive load transient is not an uncommon specification in the industry for a high performance DG unit.

Consider the following cases of weighting scalars below.

Case 1: w_p=0.5, w_s =5×10^5, and $w_{SH} = w_S$
Case 2: w_p=0.1, w_s =5×10^5, and $w_{SH} = w_S$
Case 3: w_p=0.05, w_s =5×10^5, and $w_{SH} = w_S$
Case 4: w_p=0.005, w_s =5×10^5, and $w_{SH} = w_S$
Case 5: w_p=0.0001, w_s =5×10^5, and $w_{SH} = w_S$

In all the cases above, equal weighting scalars are applied to the fundamental compensator states and the harmonic states ($w_{SH} = w_S$), while the plant states weighting w_p in each case is decreased from 0.5 all the way down to 0.0001. The time response simulations for Case 1 is illustrated in Fig. 9 showing the output voltage, reference voltage, load current, and RMS variation of the output voltage during both 0 to 100% and 100% to 0% resistive load transients. From Fig. 9 it can be seen that the output voltage RMS deviates as much as close to 20% for Case 1.

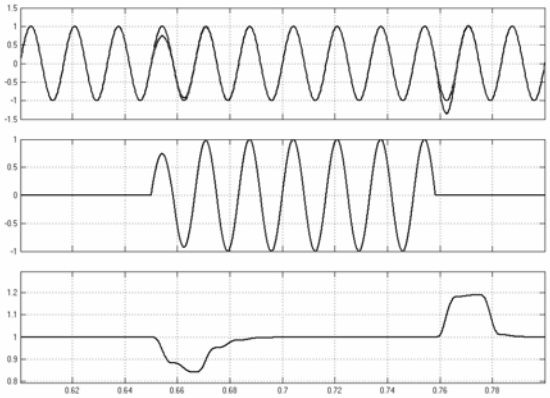

Fig. 9 Transient response for Case 1: w_p=0.5, w_s =5×10^5, and $w_{SH} = w_S$. The top trace is the output voltage and its reference, the middle trace is the load current, and the bottom trace is RMS variations of the output voltage, all versus time (sec.).

The time response similar to Fig. 9 was obtained for each of the cases 1 to 5 and the resulting RMS output voltage variations are plotted collectively in Fig. 10. It can be seen that as the scalar weighting w_p decreases, the transient performance improves, with the RMS variation as little as 2% for the case w_p=0.0001. These results are not unexpected since the weighting scalars represent the penalty applied to each state in the system. Intuitively, decreasing w_p while keeping the compensator states weighting the same, decreases the penalty cost applied to the plant states in the cost function to be minimized. This results in allowing the plant states to move more freely and hence faster response. Notice, however, that only Case 4 and Case 5 results in RMS variations of less than 5%.

To analyze the robust stability, the upper bound of the structured singular value in each case is plotted in Fig. 11. It can be seen that only Case 1, Case 2, and Case 3 achieve robust stability under the considered structured perturbations with the peak value of $\mu_\Delta(M(j\omega))$ in each case being less than 1. Case 4 and case 5 --the only cases with acceptable transient performances-- do not achieve robust stability with the peak values of $\mu_\Delta(M(j\omega))$ being 1.1 and 4 respectively.

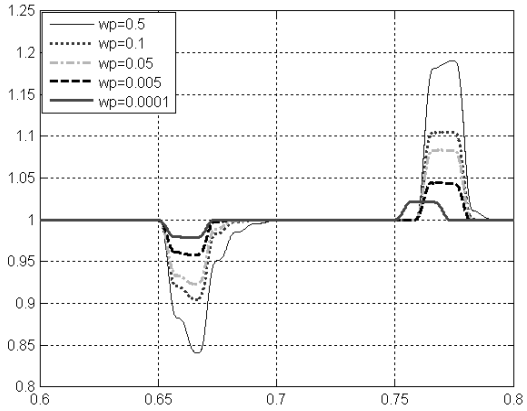

Fig. 10 RMS output voltage variations during 0 to 100% and 100% to 0 for different w_p, and $w_{SH} = w_S$.

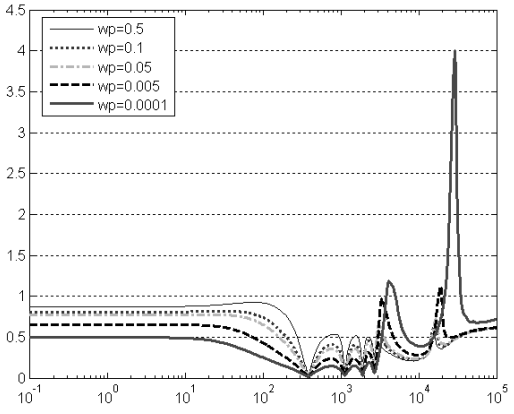

Fig. 11 Upper bound of the structured singular values for different w_p, and $w_{SH} = w_S$.

Consider now the following cases of scalars weighting:

Case 6: w_p=0.5, w_s =5×10^5, and w_{SH} = 0.01×w_S
Case 7: w_p=0.1, w_s =5×10^5, and w_{SH} = 0.01×w_S
Case 8: w_p=0.05, w_s =5×10^5, and w_{SH} = 0.01×w_S
Case 9: w_p=0.005, w_s =5×10^5, and w_{SH} = 0.01×w_S
Case 10: w_p=0.0001, w_s =5×10^5, and w_{SH} = 0.01×w_S

In the cases 6 to 10 the w_P is assigned the same value as in Cases 1 to 5 respectively, but smaller weighting is used for the harmonic compensator states as compared to the fundamental's. Fig. 12 shows the RMS variations for all cases. Comparing Fig. 10 and Fig. 12, it can be seen that the transient response improves for each of the last 5 cases, with Case 9 and Case 10 now result in only 2% and 1% RMS variations respectively.

Fig. 13 shows the upper bound of the structured singular value in Cases 6 to 10. It can be seen that reducing w_{SH} improves the stability robustness of each of the cases previously considered. The counterpart of Case 4 (Case 9)

now achieves robust stability with $\mu_\Delta(M(j\omega))$ peak value of 0.7 giving robust stability margin of $1/0.7 > 1$. Case 10 still does not achieve robust stability with peak value of $\mu_\Delta(M(j\omega))$ still greater than one.

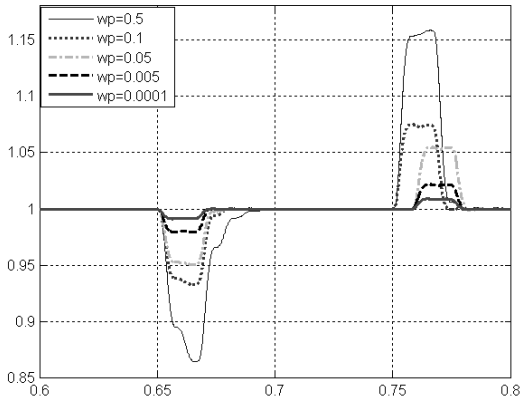

Fig. 12 RMS output voltage variations during 0 to 100% and 100% to 0 for different w_p, and $w_{SH} = 0.01 \times w_S$.

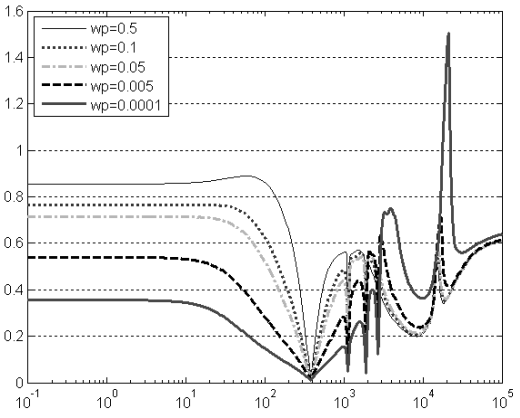

Fig.13 Upper bound of the structured singular values for different w_p, and $w_{SH} = 0.01 \times w_S$.

Comparing all the above cases, it can be seen that Case 9 gives the best transient performance while still maintaining stability robustness of the system under the structured perturbations considered.

Continuing with the analysis, it is instructive to see how each parameter perturbation affects the stability robustness of the system. For this purpose, the frequency response of each individual perturbation can be plotted as shown in Fig, 13 for the system with controller in Case 9. It can be seen from Fig. 14 that for all the perturbations, the frequency response values are less than 1.0, which confirms the stability robustness result of the structured singular value presented earlier. The inverter filter inductor has the highest peak frequency response value, with peak value of around 0.7, which means that an individual perturbation in this parameter will be the closest to the margin of making the system to be unstable. Closed loop pole-zero map of the uncertain closed loop system in Fig. 8 with all other δ 's set to zero except for the δ_{linv} can be obtained for different values of $|\delta_{linv}|$ less than 1 and greater than 1. This is illustrated in Fig. 15. The system is stable at nominal inductance value ($\delta_{linv} = 0$), $\delta_{linv} = -0.5$, and at the lowest value of the component tolerance ($\delta_{linv} = -1.0$). As the value δ_{linv} is decreased further the system finally becomes unstable at δ_{linv} slightly less than -1.4.

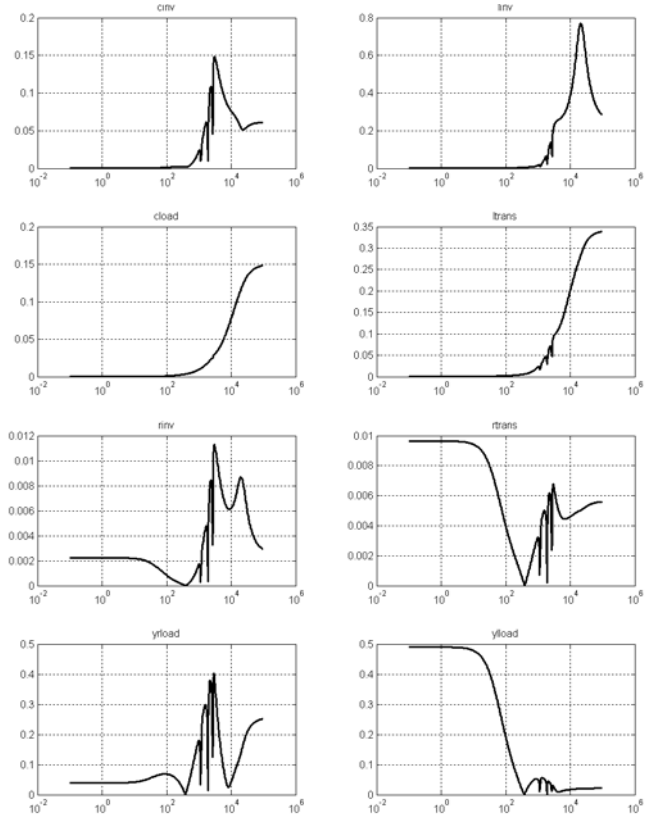

Fig. 14 Individual-perturbation frequency response for system with controller in Case 9. (X-axis in each plot is frequency in rad/sec).

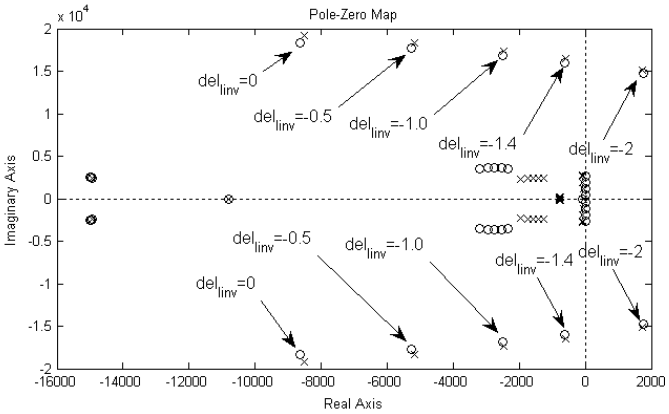

Fig. 15 Pole (x)-zero (o) map of closed loop uncertain system for different values of individual-perturbation in inverter filter inductance parameter.

V. CONCLUSIONS

The stability robustness of the control system proposed in [8] was verified using Structured Singular Value Method under structured perturbations due to component parameters

errors and linear load variations. It was shown that the scalar weighting in the optimal control cost function provides a way of tuning the transient performance of the controller while maintaining stability robustness of the system under perturbations due to plant parameter uncertainties.

REFERENCES

[1] D. Czarkowski, L. R. Pujara, and M. K. Kazimierczuk, "Robus stability of state-feedback control of PWM DC-DC push-pull converter," *IEEE Trans. Ind. Electron.*, vol. 42, no. 1, pp. 108-111, Feb. 1995.

[2] H. Ozbay, *Introduction to feedback control theory*. New York, NY, USA: CRC Press, 1999.

[3] H.A. Grundling, E.G. Carati, and J.R. Pinheiro, "Analysis and implementation of a modified robust model reference adaptive control with repetitive controller for UPS applications," *Proceedings of the 24th Annual Conference of the IEEE Industrial Electronics Society*, Aug./Sep. 1998, Aachen, Germany, vol.1, pp.391-395.

[4] T.S. Lee, K.S. Tzeng, and M.S. Chong, "Robust controller design for a single-phase UPS inverter using μ-synthesis," *IEE Proceedings-Electric Power Applications* vol. 151, no. 3, pp. 334-340, May 2004.

[5] J. L. Lin and S. J. Chen, "μ-based controller design for a DC-DC switching power converter with line and load variations," in *Proc. 22th Annual Conference of the IEEE Industrial Electronics Society* (*IECON'96*), vol. 2, Taipei, Taiwan, Aug. 1996, pp. 1029-1034.

[6] A. M. Mohamed, "Modern robust control of a CSI-fed induction motor drive system," in *Proc. 1998 American Control Conference*, vol. 6, Philadelphia, PA, USA, June 1998, pp. 3803-3808.

[7] Z. M. Ye, P. K. Jain, and P. C. Sen, "Robust controller design for high frequency resonant inverter system with voltage mode control," in *Proc. 30th Annual Conference of the IEEE Industrial Electronics Society* (*IECON'04*), vol. 1, Busan, Korea, Nov. 2004, pp. 41-46.

[8] M.N. Marwali and A. Keyhani, "Control of distributed generation systems – Part I: voltages and currents control," *IEEE Transaction on Power Electronics*, Vol. 19, No. 6, pp. 1541-1550, November 2004.

[9] M. Dai, A. Keyhani, J.W. Jung, and A.B. Proca, "A low cost fuel cell drive system for electrical vehicles," *Global Powertrain Congress'03 Conf. & Expo.*, Sept. 2003, Ann Arbor, MI, USA, Advanced propulsion strategy, pp. 22-26.

[10] R. Teodorescu and F. Blaabjerg, "Flexible control of small wind turbines with grid failure detection operating in stand-alone and grid-connected mode," *IEEE Transactions on Power Electronics*, vol. 19, no. 5, pp. 1323-1332, Sept. 2004.

[11] M. N. Marwali, "Digital Control of PWM Inverters for High performance UPS", *PhD Dissertation,* Ohio State University, Columbus, OH, December 2004

[12] E.J. Davison and B. Scherzinger, "Perfect control of the robust servomechanism problem," *IEEE Trans. on Automatic Control*, vol. 32, no. 8, pp. 689-702, Aug. 1987.

[13] B.A. Francis and W.M. Wonham, "The internal model principle for linear multivariable regulators," *Applied Mathematics and Optimization*, vol. 2, no. 2, pp. 170-194, 1975.

[14] TheMathworks, *Control System Toolbox User's Guide Version 6*, The Mathworks Inc., Natick, MA, June 2004.

[15] G.J Balas, J.C. Doyle, K. Glover, A. Packard, and R. Smith, *The μ Analysis and Synthesis Toolbox*, Mathworks, Natick, MA , 1991.

[16] R. Chiang, and M. Safonov, *Robust Control Toolbox*, Mathworks, Natick, MA, 1998.

Mohammad N. Marwali (M'98) received the B.S.E.E. degree from The Institut Teknologi Bandung, Bandung, Indonesia, in 1993 and the M.S.E.E. and Ph.D. degree from The Ohio State University (OSU), Columbus, in 1997 and 2004 respectively. He is now with Liebert Corporation in Delaware, Ohio.

His research interests are in the area of control of uninterruptible power supplies, distributed generation systems, electric motor drives, and power converters.

Min Dai (S'99) received the B.S. and M.S. degrees in electrical engineering from Tsinghua University, Beijing, China, in 1994 and 1997, respectively, and the M.S. degree in computer science from the University of Alabama, Huntsville, in 1999. He joined the Department of Electrical Engineering, The Ohio State University, Columbus, as a Ph.D. student in 1999.

His research interests include power converter control for UPS and distributed generation applications, fuel cell power conversion, electrical machines, and drives.

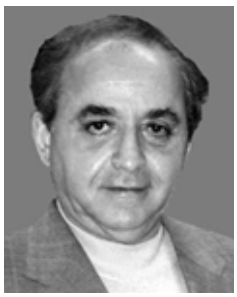

Ali Keyhani (S'72–M'76–SM'89–F'98) was with Hewlett-Packard Company and TRW Control, from 1967 to 1972. Currently, he is a Professor of electrical engineering at The Ohio State University (OSU), Columbus. He serves as the Director of OSU Electromechanical and Mechatronic Systems Laboratory. His research activities focus on the control of distributed energy systems, design and modeling of electric machine, control and design of power electronic systems, DSP-based virtual test bed for design, control of power systems, automotive systems, modeling, parameter estimation, and failure detection systems.

Dr. Keyhani received the OSU College of Engineering Research Award for 1989, 1999, and 2003. He was an Editor for the IEEE TRANSACTIONS ON ENERGY CONVERSION and past Chairman of the Electric Machinery Committee, IEEE Power Engineering Society.